Magnetism and Topology

Andre Thiaville, Jacques Miltat, Stanislas Rohart

Magnetism and Topology

André Thiaville,* Jacques Miltat, and Stanislas Rohart
Université Paris-Saclay, CNRS, Laboratoire de Physique des Solides, 91405 Orsay, France

This chapter explains what topology brings to the physics of magnetic textures in real space, from a physicist's point of view. The statics of magnetic textures is first discussed, and the distinction is made between a topological defect and a topologically stable - or protected - structure, also called topological soliton. The attention is then turned towards the physically observable consequences of topology, mainly in the dynamics of magnetic textures. Connection with experimental observations and applications is made, from early works at the beginnings of magnetic data storage up to the recent work on magnetic skyrmions, which triggered a revival of interest in topology as applied to magnetism.

I. INTRODUCTION

The application of topology to describe real-space structures in condensed matter has developed over the years, in fact as topology itself was being rigorously constructed. The first structures treated by this approach were the defects, like dislocation lines in crystal lattices, or the lines observed in liquid crystals, at the beginning of the 20th century. The methodology was then extended to structures that contain no defect. We shall keep this historical order for the first half of this chapter, dealing with the static description of magnetic structures (also called magnetic textures). The second half will deal with the dynamics of the magnetic structures.

In this chapter, mathematical formalism will be kept to a minimum. The reader completely unaware of this field of mathematics should here and there refer to textbooks [1, 2] or review papers [3] and, if a deeper mathematical view is desired, to the last chapter of this book.

Defects can appear only when there is an underlying order. In condensed matter physics there are many cases where phases with different types or degree of order appear in sequence, for example when temperature or pressure is changed. In the Landau theory of phase transitions, order is characterized by the existence of a certain physical quantity called order parameter, which can be a scalar, a complex number, a vector, a tensor, etc. This order parameter is also endowed with a certain number of degrees of freedom, defining a space V called the manifold of internal states. To be specific, let us enumerate the cases for magnetism. The order parameter is the magnetic moment. Depending on the type of magnetism (localized or itinerant), magnetic order (ferromagnetic, ferrimagnetic [Note that we do not consider in this chapter the antiferromagnets, for which the order parameter is different]), and also atomic structure (single crystal, polycrystal, amorphous), the distribution of the magnetic moment on the atomic scale will be very different. However, on the mesoscopic lengthscale where micromagnetics [4, 5] reigns, these atomic subtleties are polished out, leaving only a magnetic moment that is a continuous function of space and time. This moment has a zero thermodynamical average above the Curie temperature, and a non-zero one below this temperature, leading to a spontaneous magnetization $M_s(T)$ a sole function of temperature T. The degrees of freedom correspond to the orientation of this moment, and they are described by a unit vector $\vec{m}(\vec{r}, t)$, a function of position $\vec{r}$ and time t. Our world being three-dimensional, three cases are considered.

- *Heisenberg model:* Magnetization has $n = 3$ components as $\vec{m}$ can take any orientation in 3D, the manifold of internal states is $V = \mathbb{S}^2$, the unit sphere in three dimensions which is described by two variables (for example the polar angle θ and the azimuthal angle ϕ), hence the exponent 2. Physically this should be the only case, in general. It is however sometimes interesting to consider the two other limiting cases.

- *XY mode:* This case corresponds to an easy plane, magnetization has $n = 2$ components, the out of plane anisotropy energy being (mathematically) infinite. Physically it means that other energy terms are much smaller. This can be a description of a soft magnetic thin film, or of a weak ferromagnet (the orthoferrites, for example) where the Dzyaloshinskii-Moriya interaction confines the ferromagnetic moment to the plane normal to its vector. The manifold of internal states is $V = \mathbb{S}^1$, the unit cercle in the (easy) plane, described by just one variable (the angle).

- *Ising model:* The last case is complementary to the preceding one, with an easy axis of (mathematically) infinite anisotropy, so that magnetization has just $n = 1$ component. The manifold of internal states is $V = \mathbb{S}^0$, this notation meaning just the two points +1 and -1.

The internal space V plays a capital role in the topological formalism.

* andre.thiaville@universite-paris-saclay.fr

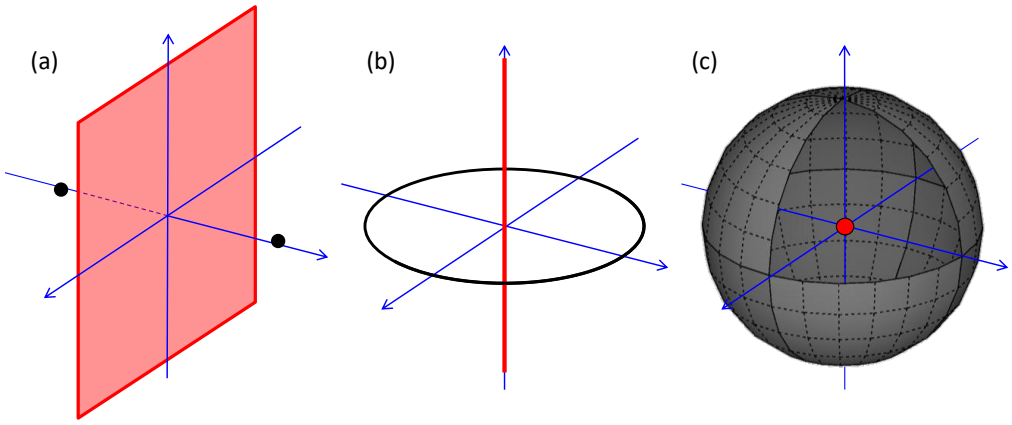

FIG. 1. The contour dimensionality r is adapted to the defect dimensionality d' according to Eq. 1, as illustrated here for (a) $d' = 2$, (b) $d' = 1$ and (c) $d' = 0$. The defects are drawn in red, and the associated contours in gray.

II. TOPOLOGICAL DEFECTS IN MAGNETISM

In a medium with order, a defect is a point or a collection of points where the order parameter is not defined; one can have a point-like defect, or a defective line, or a defective surface (etc. for space dimensions d larger than 3). The defect is said to be topological when, whatever the continuous modifications exerted on the order parameter distribution over space, it cannot be removed. In short, this defect cannot be cured.

The defect dimensionality is called $d' = 0$ for a point, $d' = 1$ for a line and $d' = 2$ for a surface. The dimension of the physical space being denoted d, one has $d' < d$. Note that the defect, in this idealization of the order parameter as a continuous function, has no width, it is just a discontinuity of the order parameter. But how can the presence or not of a defect with no size be detected ? This can be done with topology. The method is inspired by the Burgers circuit used to detect the presence of dislocation lines in atomic arrangements [6]. The generalization of this method is to consider a closed contour of dimension r in the physical space (i.e. the sphere $\mathbb{S}^r$, or any continuous deformation of it). To look for a defect of dimension d' in a space of dimension d, the contour dimension r has to satisfy[7, 8]

$$d' + r + 1 = d. \tag{1}$$

The case of a dislocation line ($d' = 1$) in the usual space with $d = 3$ corresponds to a closed loop $r = 1$. Similarly, to look for a point defect $d' = 0$ in the 3D space ($d = 3$) requires a sphere-like surface hence $r = 2$ (Fig. 1).

Every magnetization texture, by the orientation of the magnetization vector, gives rise to an image of the r-dimensional closed contour on the parameter space V. In mathematical terminology this is called a mapping. A continuous deformation of the magnetization texture leads to a continuous deformation of the image on the parameter space V. The branch of topology called homotopy precisely deals with that. Two images are said to be equivalent (belonging to the same homotopy class) if they can be continuously transformed one into the other. For every space V there exists an object called the r-th homotopy group, denoted $\pi_r(V)$, and each element of the group is a homotopy class. The group has an obvious 'zero' (it is called neutral) element, the class of the contours whose image is a point. The group is said to be trivial if it consists only of the neutral element. This means that all contours can be continuously contracted to a point. In that case, there can be no topological defect of dimension $d' = d - r - 1$. Indeed, there will be no obstacle in shrinking in the physical space the r-dimensional contour, magnetization will be always defined on the contour, and will finally converge to the magnetization vector at the center of the contour when its size reaches zero. The topologically interesting case is the non-trivial one, when the homotopy group has more than one element. In that case, if a contour has an image on V which belongs to a non-neutral homotopy class, when shrinking this contour in physical space, at some moment the magnetization orientation has to be undefined: the defect will be met.

For the case of magnetism where $V = \mathbb{S}^{n-1}$, with n the number of magnetization components (see Sec. I), the non-trivial homotopy groups with $r < 3$ are

- $\pi_0(\mathbb{S}^0) = \mathbb{Z}_2 \equiv \{0, 1\}$: for Ising spins, there exist topological defective surfaces in 3D, topological line defects in 2D, and topological point defects in 1D;
- $\pi_1(\mathbb{S}^1) = \mathbb{Z} \equiv \{0, +1, -1, +2, -2, ...\}$: for XY spins, there exist topological linear defects in 3D space, and topological point defects in 2D;
- $\pi_2(\mathbb{S}^2) = \mathbb{Z}$: for Heisenberg spins, there are topological defects in the form of points in 3D space.

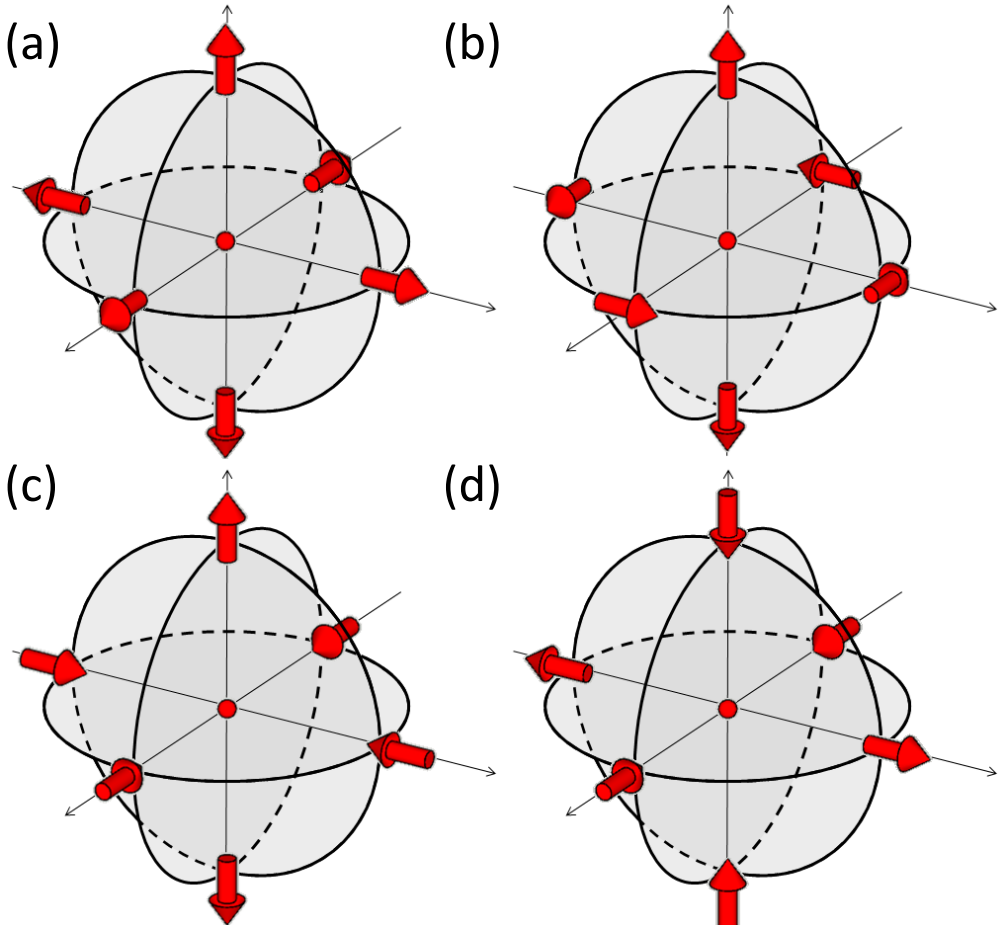

FIG. 2. The orientations of the magnetization on a sphere surrounding the Bloch point are schematically drawn. (a) so-called hedgehog Bloch point, with radial magnetization everywhere, covering the unit sphere +1 time. The variant with opposite magnetization everywhere covers the unit sphere −1 time, so is topologically different. (b) so-called combed Bloch point, with a lower magnetostatic energy [10], which is found in most structures (see Sec. V). This structure can be derived from (a) by a $\pi/2$ rotation of the magnetizations around the vertical axis, hence is topologically equivalent. (c) structure derived from (a) by a π rotation around the vertical axis, so again topologically equivalent to it. (d) structure which has a $S = -1$ winding number on the equator, with a $p = -1$ axial magnetization on the poles, hence also covering +1 time the sphere. It is also the same as (c), rotating the whole sample by $\pi/2$ around a horizontal axis.

The well-known examples of the second case are the Kosterlitz-Thouless vortices and antivortices (Fig. 3), whereas in the third case it is the Bloch point (Fig. 2). Therefore, given that the XY and Ising models are only approximations, the only true topological defect in ferromagnetism is the Bloch point.

A. The Bloch point

The structure and the name were invented by Ernst Feldtkeller in Ref. [9], a pioneering paper for the application of topology to magnetism. It is the first topological magnetic structure studied; it has the defining property that around it every magnetization orientation appears once exactly. Some schematic structures of the magnetization around it are drawn in Fig. 2

A surprising property of the Bloch point is that it has a finite energy. In the frame of micromagnetics, even if the exchange energy density diverges like A/r^2 around the Bloch point [A is the micromagnetic exchange constant, proportional to the exchange energy J and inversely proportional to the lattice constant. [5]], the integral of this density is finite, amounting to $8\pi AR$, R being the radius up to which the Bloch point profile holds. On the other hand, going back to the atomic scale, having a Bloch point amounts to forcing to zero the magnetization in a volume of the size of an atom. Thus, if J is the exchange energy per nearest-neighbor bond, and Z is the number of nearest neighbors, the cost of a Bloch point is about ZJ. For a simple cubic lattice, the two formulae are close for $R = a/2$. This is the 'core' cost of a BP, consisting of exchange only.

The magnetostatic cost of a Bloch point was evaluated by W. Döring [10]. It was found that the hedgehog Bloch point

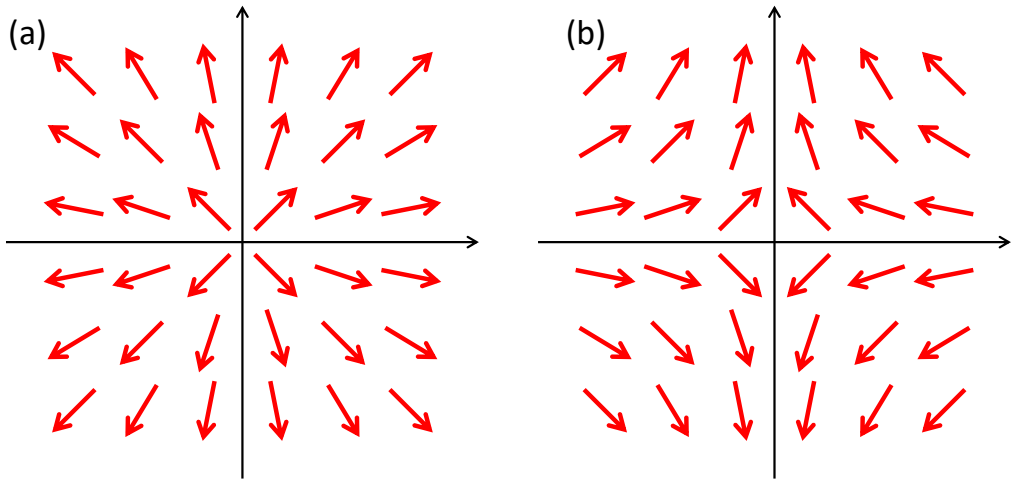

FIG. 3. The orientations of the magnetization around the vortex core, located at the origin, are figured by arrows. (a) Vortex, here in the radial variant. This structure can be continuously converted into the circulating variants (like the velocity field of a vortex in fluid dynamics), with both circulation directions. All these variants are described by the constant C in the relation $\phi = \varphi + C$, with φ the angle of the position vector, and ϕ the angle of the magnetization. (b) Antivortex, described by $\phi = -\varphi$ (any additional constant can be absorbed by a rotation of the coordinate axes).

(Fig. 2(a)), being a monopole, has the highest energy. Conversely, the 'combed' Bloch point (Fig. 2(b)) carries much less energy. There is also an anisotropy cost of a Bloch point. Altogether, the insertion energy of a Bloch point in a material with anisotropy (K) dominating magnetostatics is given by a micromagnetic radius $R \approx \sqrt{A/K}$ [11].

In the framework of atomic micromagnetics, the exchange energy cost as a function of the position of the mathematical center of the Bloch point (in between the atoms) was studied by Reinhardt, who found the best interstitial positions for the Bloch point as well as its saddle point when moving from an atomic cell to another [12]. The friction linked to these saddle points was shown to be detectable in the motion of so-called Bloch point walls in nanowires [13].

B. The singular vortex

As is apparent from Fig. 3, a vortex topological point defect for the XY model (therefore in 2D) can be seen as a cut through the center of a Bloch point, the point topological defect for the Heisenberg model, so in 3D.

Regarding the vortex energy, the exchange energy density in the continuous micromagnetic formulation diverges again as A/r^2, but now the radial integral also diverges logarithmically [14]. The divergence at small size is removed, in the theory papers, by introducing a finite lower bound for the integration over the radius. This indeed corresponds to the atomic micromagnetic calculation, which gives a finite result.

III. TOPOLOGICALLY STABLE STRUCTURES (TOPOLOGICAL SOLITONS) IN MAGNETISM

In the same pioneering paper by E. Feldtkeller [9], another topological effect relative to the magnetic structures was introduced. Consider a regular magnetic structure, i.e. without any defect, as well as another structure, also without defect. The question is whether or not it is possible to continuously transform one structure into the other (a property called accessibility). This is again a topological question. It is not at all academic, as E. Feldtkeller was considering the possible obstacles to the magnetization reversal in ferromagnetic rings, used as bits in the ferrite core memory.

When it is not possible to transform continuously one structure into another, the structures are said to be topologically stable or, equivalently, they are called topological solitons [15]. The idea behind the latter name is that, similarly to a soliton that keeps its shape while moving, a topological soliton keeps its topology while deforming (moving being one way of deforming).

In order to apply homotopy arguments to this situation, we need to realize mappings from r-dimensional spheres $\mathbb{S}^r$ to the order parameter space V. A perfect case is therefore when the sample itself is a sphere, like a film grown on a sphere realizing $\mathbb{S}^2$, or a nanoring realizing $\mathbb{S}^1$. The first case is rare presently, it could be realized by core-shell magnetic particles with large diameter. The second case has been studied in detail [16], but the magnetic structures (domain walls) are the same as when the nanoring is not closed, discussed in Sec. III B 3.

A. Uniform boundary conditions

If the physical space is the infinite euclidian space $\mathbb{R}^d$, we cannot directly apply homotopy arguments as $\mathbb{R}^d$ is not equivalent to $\mathbb{S}^d$, even if they have the same number of dimensions. But if, in addition, it is known that magnetization is uniform at infinity, then by a transformation similar to the stereographic projection of the sphere onto the plane, one can transform $\mathbb{R}^d$ to $\mathbb{S}^d$.

In such situation we see that all magnetic structures realize mappings of $\mathbb{S}^d$ to the order parameter space V. So they can be classified by the homotopy group $\pi_d(V)$. Let us be more explicit by specifying d, for $V = \mathbb{S}^{n-1}$ (except the case corresponding to $\pi_0(\mathbb{S}^0) = \mathbb{Z}_2$ that is not interesting).

1. *Two-dimensional physical space ($d = 2$)*

This case is non trivial as $\pi_2(\mathbb{S}^2) = \mathbb{Z}$. This means that the physical space is bi-dimensional (one can think of a film where nothing changes along the thickness, for example an ultrathin film with a thickness not much above the magnetic exchange length $\Lambda = \sqrt{2A/\mu_0 M_s^2}$). So topology tells us that for 3D moments ($n - 1 = 2$) on a plane, which are uniform at infinity (i.e. the structures considered are of finite extent), there exists an infinity of topologically different structures, labelled by the signed integers (called the topological index). Two structures with different index are mutually inaccessible by continuous deformation. Among these structures, only those with index zero can be continuously transformed to the uniform state. The simplest structures are drawn in Fig. 4. The structure with index +1 is called a skyrmion, that with index -1 an antiskyrmion, and the others are higher order skyrmions.

The topological index is easy to calculate in this situation, as it is simply the number of times that the sphere $\mathbb{S}^2$ is covered by the mapping. If the plane $\mathbb{R}^2$ is described by (x, y) coordinates, we see from geometry that the differential surface covered on the sphere reads

$$d\Omega = \left(\frac{\partial \vec{m}}{\partial x} \times \frac{\partial \vec{m}}{\partial y} \right) \cdot \vec{m} \, dxdy. \tag{2}$$

Indeed, $\vec{m}$ is the local normal to the sphere, both partial derivatives of $\vec{m}$ belong to the local tangent plane to the sphere, the modulus of their vector product is the sine of their angle, which is giving the surface of the associated parallelogram. Note that the covered surface can be positive or negative. Altogether, the topological index is the integral of $d\Omega$, divided by 4π which is the surface of the sphere. It is notable that, here, the topological index can be obtained by the space integral of a 'topological density'.

In the case of cylindrical symmetry, namely $\vec{m} = (\sin\theta\cos\phi, \sin\theta\sin\phi, \cos\theta)$ with the spherical angles θ and ϕ relative to the magnetization at infinity being sole functions of the radius r and the in-plane angle φ, respectively, one obtains the useful relation

$$\Omega = \int \sin\theta \frac{d\theta}{dr} dr \int \frac{d\phi}{d\varphi} d\varphi = 4\pi S \, p. \tag{3}$$

The two quantities involved are $p = [\cos\theta(0) - \cos\theta(\infty)]/2$, the polarity of the core of the structure, and $S = \int_0^{2\pi} \frac{d\phi}{d\varphi} d\varphi/(2\pi)$, the winding number of the planar magnetization component. Note that, if the structure considered does not possess cylindrical symmetry, it can be continuously deformed so as to show it. This formula is therefore general.

2. *One-dimensional physical space ($d = 1$)*

This is another non trivial case, due to the fact that $\pi_1(\mathbb{S}^1) = \mathbb{Z}$. The physical space is now one-dimensional (a nanowire), the moments are XY ($n - 1 = 1$), and they are identical at both ends, so that the wire can be thought as a closed loop. A physical realization of this situation could for example be a nanowire where the moments are constrained to lie in the transverse plane, so that a magnetic structure is locally a helix. In this case, the topological index is simply the algebraic number of turns of the helix. Another realization of this situation could be an ultrathin film (normal to z) where the moments vary only along one direction x (e.g. a series of parallel domain walls). Then again we could have helices (moments in the (y, z) plane), or also cycloids (moments in the (x, z) plane), these planes being fixed by a strong Dzyaloshinskii-Moriya energy term. The topology is the same for both realizations.

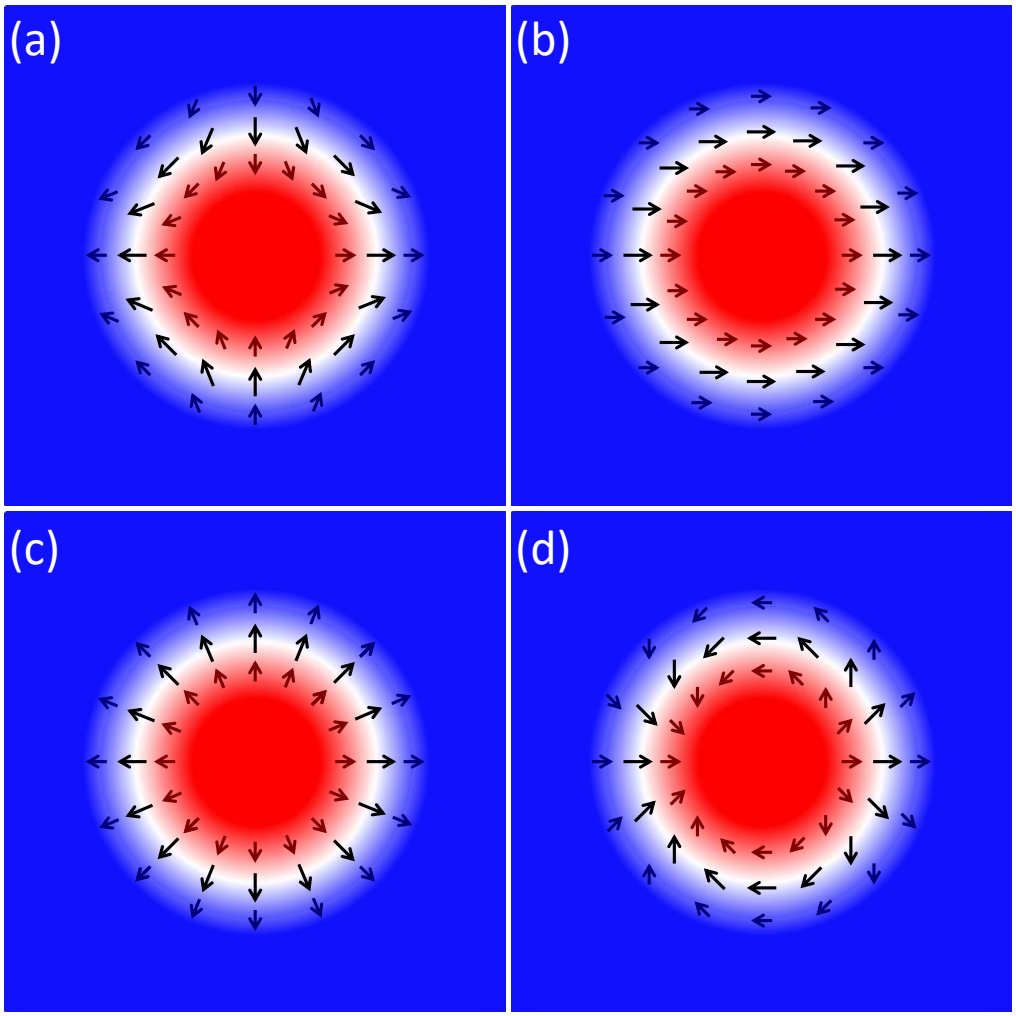

FIG. 4. The in-plane components of the magnetization are depicted by black arrows, whereas the out of plane component is coded in color (blue=down, red=up, white= in-plane). (a) anti-skyrmion with an in-plane winding number $S = -1$. (b) non-topological structure with an in-plane winding number $S = 0$. This structure can be continuously destroyed by a magnetization rotation around the vertical in-plane axis, the angle of rotation being π at the center, $\pi/2$ at the wall and 0 at infinity. (c) a Néel skyrmion with positive chirality. Note that, by π rotation of the moments around the perpendicular axis, this structure can be continuously transformed into a Néel skyrmion with negative chirality, as well as into Bloch skyrmions with positive or negative chirality by $\pm\pi/2$ rotation. (d) a higher order skyrmion with an in-plane winding number $S = +2$.

3. *Three-dimensional physical space ($d = 3$)*

There exists also $\pi_3(\mathbb{S}^2) = \mathbb{Z}$. Whereas the previous homotopy groups were rather intuitive, this one is not. It was only reported in 1931 by the mathematician Heinz Hopf [17], and a mapping of $\mathbb{S}^3$ to $\mathbb{S}^2$ is called a Hopf fibration, the name fiber coming from the fact that each point on $\mathbb{S}^2$ is the image of a line of points in $\mathbb{S}^3$, a fiber. By the same argument as before, $\mathbb{S}^3$ is $\mathbb{R}^3$, just with identical moments at infinity, i.e. we discuss finite three-dimensional magnetic structures within a uniform background.

The structures with index 1 are now called hopfions; they have been observed in hybrid magnetic liquid crystals [18] and predicted in nanostructures of non-centrosymmetric magnets [19]. The topological index was described by Hopf, it is the linking number between any two fibers. It can also be calculated by integration of a density, albeit non-local [20], related to the presently much studied Berry curvature [21].

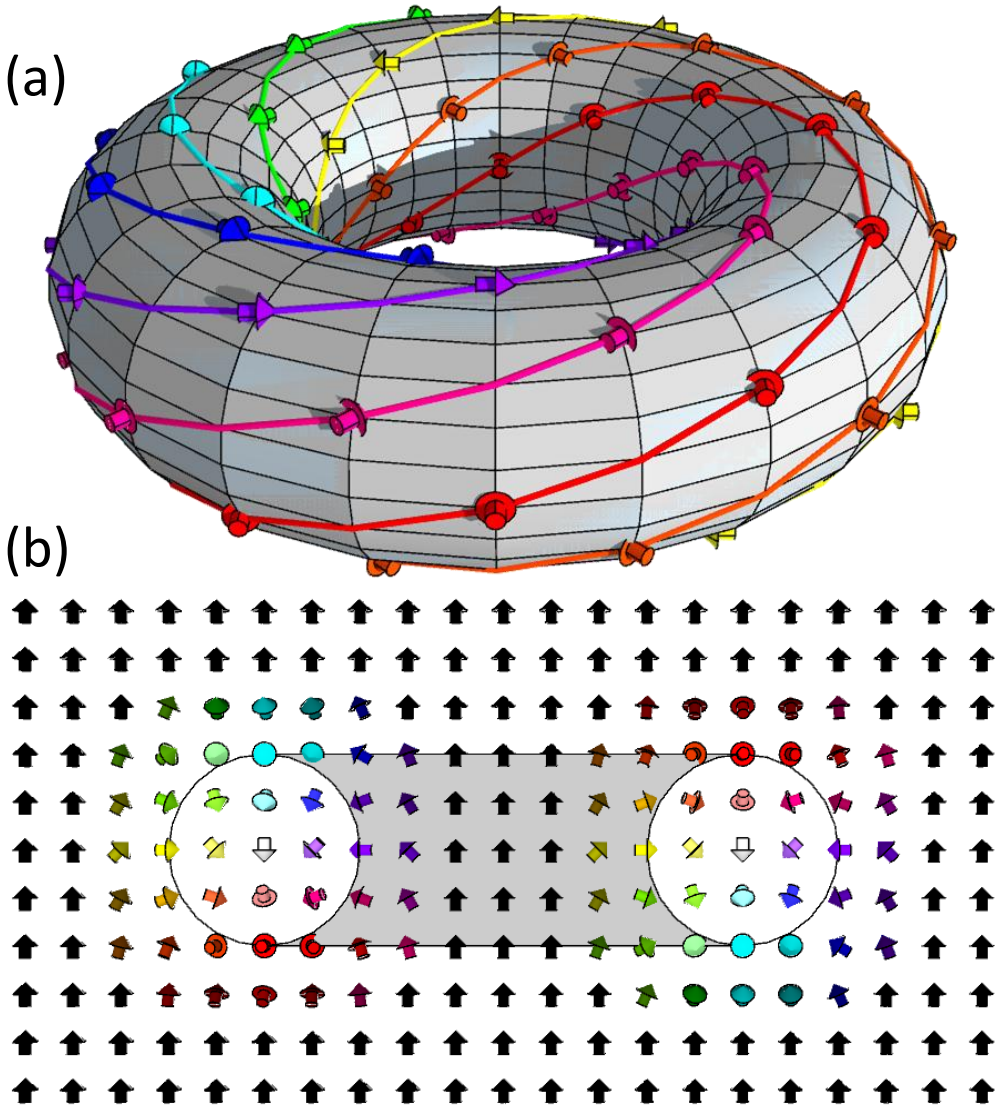

FIG. 5. (a) perspective view. The grey torus figures the locus of the in-plane oriented moments (the 'wall' of the hopfion). The orientation of magnetization on this surface is depicted by arrows, the loops with the same color drawing the fibers of the structure, the loci of the points with the same magnetization. These loops are all linked once, this being the topological index of the structure. (b) cut view through a vertical plane, with the cut of the torus superposed, allowing to see the magnetization inside the torus, which is akin to a reverse domain.

B. Non-uniform boundary conditions

Non-uniform boundary conditions are frequent. The obvious case is the domain wall, where on both sides magnetization goes to different limits at infinity. Finite samples (like patterned microstructures) are another case, the boundary conditions being imposed by the energetically preferred magnetization orientations at the edges. Two emblematic cases of this are the disk, and the nanostrip.

When additional constrains on the order parameter exist at the edge, another mathematical object exists, called the relative homotopy group. However, as the emphasis of this chapter is physics rather than mathematics, we shall directly see the consequences of the boundary conditions, case by case.

1. The domain walls

If it is enforced that magnetization goes to $\vec{m}_1$ at $x \to -\infty$ and to a different $\vec{m}_2$ at $x \to +\infty$, then a domain wall has to exist. In topological terms, it means that all paths in physical space connecting $x = -\infty$ to $x = +\infty$ have to go through $\vec{m}_1$ and $\vec{m}_2$, so

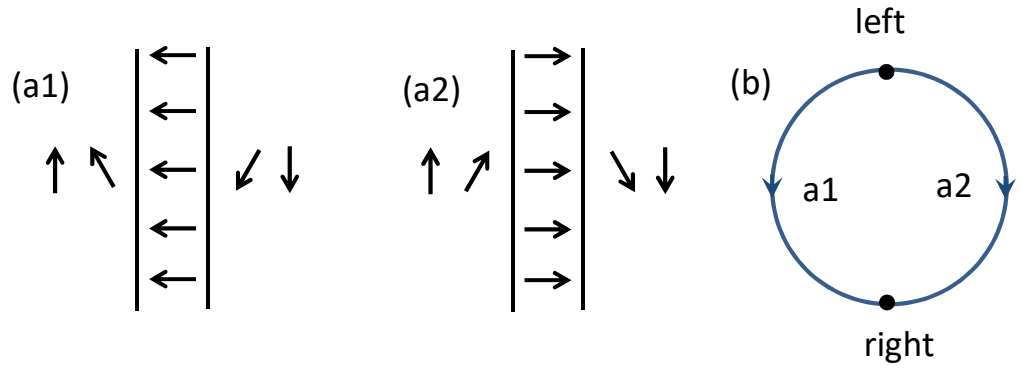

FIG. 6. (a) Two Néel walls with opposite rotation sense, between the same domains, cannot be converted continuously one into the other, if the magnetization in the domains is assumed to be fixed, as the moments are XY. (b) Corresponding paths on the unit circle $\mathbb{S}^1$. For Heisenberg moments, path $a2$ can be transformed to path $a1$ by going over a pole, above or below the plane of the drawing.

that they cannot be contracted to a point: a domain wall has indeed to exist. But we learn nothing by this tautology.

The more interesting question is whether all walls satisfying this condition can be continuously transformed one into the other. This depends on the nature of the first homotopy group of the order parameter space $\pi_1(V)$: if it is trivial then all these walls are topologically equivalent, but if it is not then topologically different walls exist. The latter case occurs for the XY model only (Fig. 6).

2. *The vortex in a soft magnetic film*

In a soft magnetic film, the demagnetizing energy dominates the anisotropy term, so that magnetization is confined to the plane of the film. A perfect confinement would mean the XY model, for which we have seen that topological defects (the vortices, antivortices, etc.) exist for $d = 2$, the present case. As confinement is not perfect in usual samples (finite magnetization, non-zero exchange), these topological defects are regularized by having the core magnetization 'escape' in the third dimension, over a size proportional to the micromagnetic exchange length $\Lambda = \sqrt{2A/(\mu_0 M_s^2)}$ (see Ref. [5, 22] for an analytic calculation of the vortex core profile in the limit of vanishing sample thickness). The question then is: are these structures topologically stable ?

The answer is Yes, if the magnetization is assumed to stay perfectly in the plane at infinity. In such a case, similarly to the plane-to-sphere transformation of Sec. III, the situation is the same as a finite disk with magnetization assumed to belong to the plane at the disk edge.

Let us look at the edge structure first. It realizes a mapping of $\mathbb{S}^1$ (the edge) to $\mathbb{S}^1$ (the equator on the unit sphere, the locus of the in-plane magnetic moments). So this structure is classified by $\pi_1(\mathbb{S}^1) = \mathbb{Z}$: it is topologically stable regarding the relevant topological index, which is the winding number of the in-plane magnetization. Thus, from the winding number of the (in-plane) edge magnetic structure, we know if we have a vortex ($S = +1$), an antivortex ($S = -1$), nothing ($S = 0$), or more complex vortices or antivortices ($|S| > 1$). Physically, as the edge constrain arises from magnetostatics, the avoidance of surface magnetic charges dictates that $\vec{m}$ be tangent to the edge. So, for a disk-shape sample, the stabilized winding number is 1.

As we have 3D spins inside the disk, the core of the vortex is not singular, but regular with a purely out-of-plane moment $m_z \equiv p = \pm 1$, p being called the polarity of the vortex. From the topology of the edge magnetization, we already know that the vortex cannot be continuously erased into a uniform structure. But could we continuously go from $p = +1$ to $p = -1$? The answer is No. Indeed, if this were the case, one would at some moment have the top surface of the film with $p = 1$, and the bottom one with $p = -1$. Then mapping the full surface of the disk (the top surface, glued to the bottom surface at the disk edge), which is like $\mathbb{S}^2$, to the parameter space $V = \mathbb{S}^2$ would give a full coverage, meaning that the disk contains a Bloch point in its interior: continuity would be broken.

We thus see that additional constrains at the sample edge let other topologically stable structures appear. As they cover half of the sphere, the Heisenberg vortex or antivortex are also called merons. Note that this half-integer coverage index of $\mathbb{S}^2$ is not quantized: if a perpendicular field is applied to a disk with a vortex, the image of the edge on $\mathbb{S}^2$ leaves the equator, increasing or decreasing the coverage depending on the field direction with respect to the core polarity (see Ref. [23] for an experimental demonstration).

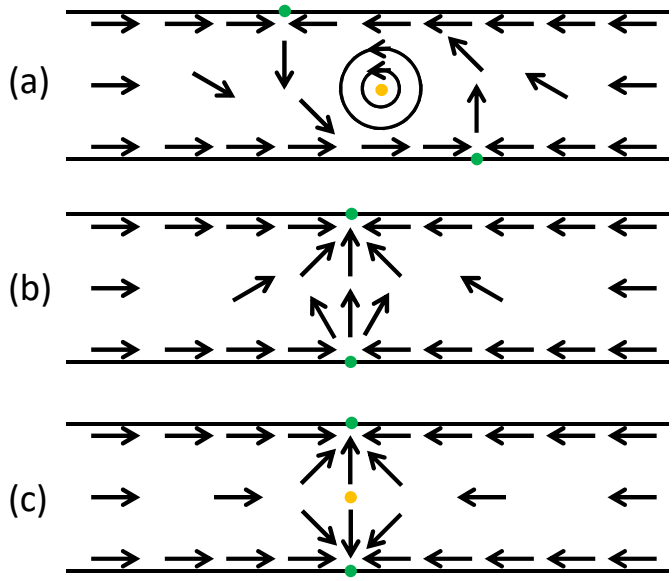

FIG. 7. (a) the vortex wall; (b) the (symmetric) transverse wall; (c) the symmetric transverse wall during its dynamical reversal of the transverse moment. The green points at the edge correspond to topological defects of $\pi_0(\mathbb{S}^0)$ (the edge when tangential magnetization is assumed), which become merons of $\pi_1(\mathbb{S}^1)$ (the edge when planar magnetization is assumed, with values fixed at infinity). The orange points correspond to topological defects of $\pi_1(\mathbb{S}^1)$ (in-plane moments assumed in the sample), which become merons of $\pi_2(\mathbb{S}^2)$ (Heisenberg spins, with in-plane spins far from the core), namely a vortex (a) and an anti-vortex (c).

3. The soft magnetic nanostrips

This case illustrates nicely how the topological objects transform when one progressively lifts the constrains on the magnetization orientation. The topological description provides a general scheme to understand the magnetic structures in the soft nanostrips [24, 25]. It has led to insightful 'mechanical' models of the domain walls in these samples [26].

The nanostrip geometry is similar to the disk case, but now the edge is not closed. At an edge, combining the magnetostatic conditions of planar magnetization for the film and tangent magnetization at the edge, one obtains that the lowest energy magnetizations are in $\mathbb{S}^0$. From the fact that $\pi_0(\mathbb{S}^0) = \mathbb{Z}_2$, there exists one associated type of topological point defect, which is just a wall in the edge magnetization.

These topological defects are regularized by lifting the tangency constrain, i.e. by considering, at the edge, $V = \mathbb{S}^1$ instead of $\mathbb{S}^0$. Assuming that the magnetization in the two domains separated by the wall is fixed (see Sec. III B 1), the topological defects of $\mathbb{S}^0$ become topological solitons, in fact merons of $\pi_1(\mathbb{S}^1)$.

Going one step further, by comparing the topological characters of the two edges (which is easy to do e.g. when, on the left and right of the nanostrip area considered, it is known that magnetization is uniform), one can know if there exists a topological defect of $\pi_1(\mathbb{S}^1)$ inside. The typical cases are the vortex wall (with a vortex inside), the transverse wall (no vortex inside), the transverse wall in the process of reverting (with an antivortex inside), see Fig. 7.

4. The vertical Bloch line

The vertical Bloch line (VBL) is the second magnetic topological object studied, and it is a topological soliton. Lines in the domain walls of garnet films were intensively studied in the 70's, in the wake of research about the bubble memories. These samples are single crystals of (at that time) few-micron thickness, epitaxially grown on a single crystal non-magnetic garnet substrate. As the lattice parameters can be precisely matched, the crystalline defect density is extremely low (1 cm between dislocations, typically). The samples are, however, not perfectly uniform magnetically as the large unit cell of garnets (a cube of 1.3 nm edge) accommodates many substituants, whose concentration can vary from place to place. The magnetic garnets are also ferrimagnetic (in fact, ferrimagnetism was discovered in the garnets), with a tunable low magnetization density. They have a growth-induced perpendicular anisotropy originating from the atomic ordering of the substituants during the growth. The magnetic structure consists of parallel domain walls with a globally disordered structure, with as limiting cases the straight parallel domains array and the bubble lattice.

As the sample thickness (few micrometers) is much larger than the domain wall width (a few tenths of a micrometer), in the

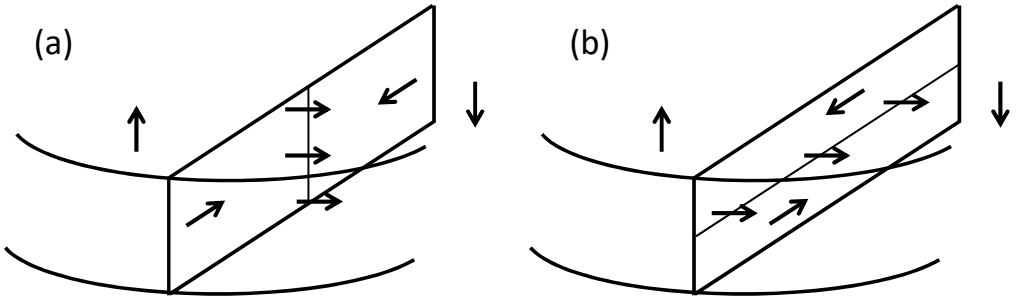

FIG. 8. The schematic drawings (perspective view) show (a) a vertical Bloch line, and (b) a horizontal Bloch line. The tilt of the domain wall magnetization at the surfaces, from a Bloch to a chiral Néel orientation, due to the stray field of the domains and that occurs in films thick enough compared to the exchange length [27], is not drawn. The lines can be magnetized in both directions. Only the vertical Bloch line is stable in statics.

(111) epitaxy case with small in-plane anisotropy one gets Bloch walls. In the vicinity of the surfaces they turn to the Néel orientation due to the stray field of the domains (twisted Néel-Bloch-Néel structure, [27]).

In turn, these walls can contain the two orientations of the Bloch wall, being separated by a line (a 'wall in a wall'). This line has its magnetic moment oriented along a Néel direction, hence the proposition by E. Feldtkeller to call them Néel lines. But lines in domain walls had been observed earlier in soft thin films supporting Néel walls, and called Bloch lines, so that this generic name was kept for all types of lines. As shown in Fig. 8, in a garnet film horizontal Bloch lines (HBL) and vertical Bloch lines (VBL) exist. The HBL is an intermediate state during the dynamics, whereas the VBL is a stable structure. Moreover, in the 80's a Bloch line memory was developed, taking advantage of the properties, including the topological ones, of the VBLs [28]. So we concentrate on VBLs here.

The topological stability of a VBL within a domain wall is analyzed similarly to the case of the vortex. Magnetization is fixed in the domains far from the wall, as well as in the wall far from the VBL, so that in fact far away (in 2D) from the VBL magnetization is fixed. In the absence of fields transverse to the easy axis, these fixed magnetizations belong to a great circle on $\mathbb{S}^2$, so that the VBL is also a meron of $\pi_2(\mathbb{S}^2)$.

C. Role of topological defects for topological solitons

The preceding sections have shown relations between topological defects and topological solitons. These can be seen by comparing the situations described by the same homotopy group. Take $\pi_2(\mathbb{S}^2)$ as a start. It describes topological point defects in a 3D medium, as well as topological solitons for a 2D medium, both cases being for Heisenberg spins. The relation is simple: in the transformation from a topological soliton to a different one, the breaking of continuity is realized by the presence of a topological defect corresponding to the difference of their topological indices. In this comparison, one goes from a 2D medium to a 3D one either by time-stacking the 2D media, or by considering the different slices of its thickness. For example, annihilating a skyrmion requires a Bloch point. Two examples of this are the merging of two skyrmions [29], and the so-called 'bobber' structure where a skyrmion exists in the vicinity of one surface of the film only, a Bloch point terminating the structure [30].

Similarly, $\pi_1(\mathbb{S}^1)$ describes topological point defects (vortex, antivortex, etc.) in a 2D medium and for XY spins, as well as topologically stable knots of these spins along a line. Going from a line with one knot to a line without knot requires, similarly, a vortex or an antivortex (see Fig. 9).

IV. EFFECT OF TOPOLOGY ON MAGNETIZATION DYNAMICS

Up to now we have discussed the statics of magnetic structures. As we are going to show in this section, the dynamics of magnetic structures is also affected by topology, in some cases.

In general, magnetization dynamics in continuous media is governed by the Landau-Lifshitz-Gilbert (LLG) equation [5, 31, 32], supplemented by additional torque terms in presence of spin-polarized currents [33, 34]. In this equation, the energy density $\mathcal{E}$ gives rise to an effective magnetic field $\vec{H}_{\text{eff}}$ defined by a variational equation [31]. [Following the use of the magnetic CGS system in the older literature, one continues to use the name of an effective field, hence the μ_0 factors appearing at (too) many places. It would be simpler to employ the effective induction $\vec{B}_{\text{eff}} = \mu_0 \vec{H}_{\text{eff}}$, but for homogeneity with the other chapters of this

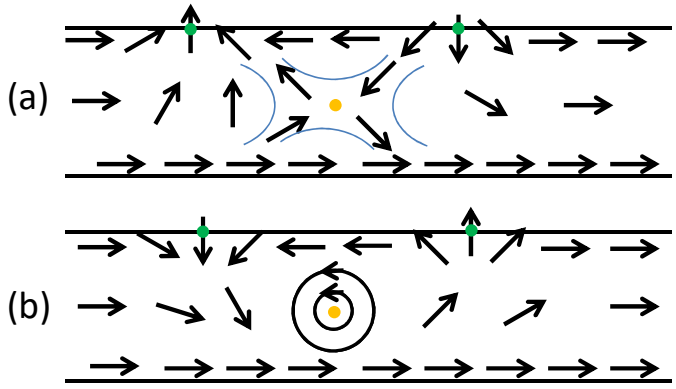

FIG. 9. Soft magnetic strip where on the lower edge magnetization is uniform, whereas on the upper edge it makes a 2π turn, one way (a) or the other (b). For XY moments, the 4 sides of the structures drawn constitute a closed path, on which the moments turn by -2π (a) or $+2\pi$ (b). Hence there must be a topological defect of $\pi_1(\mathbb{S}^1)$ inside, the antivortex (a) or the vortex(b). For Heisenberg moments, if we assume that moments far away are in the plane, the structures are topological solitons (merons) of $\pi_2(\mathbb{S}^2)$.

book we will use the effective field.]

$$dE \equiv \int d\mathcal{E} = -\mu_0 M_s \int \vec{H}_{\text{eff}} \cdot d\vec{m}. \tag{4}$$

The LLG equation then reads

$$\frac{\partial \vec{m}}{\partial t} = \gamma_0 \vec{H}_{\text{eff}} \times \vec{m} + \alpha \vec{m} \times \frac{\partial \vec{m}}{\partial t} + \frac{\gamma_0}{\mu_0 M_s} \vec{T}. \tag{5}$$

In this equation $\gamma_0 = \mu_0 \|\gamma\|$ is the gyromagnetic factor as adapted to fields, with the negative sign of the electron charge absorbed in the reversal of the vector product, α is the dimensionless damping coefficient as introduced by Gilbert [32, 35], and $\vec{T}$ represents the current-induced torques (spin transfer torques [36], spin-orbit torques [37]), as generally they do not derive from an energy density. As the effective field has contributions from the energy densities of exchange, magnetic anisotropy, applied field, demagnetizing field as well as Dzyaloshinskii-Moriya anti-symmetric exchange etc., this equation is quite complex and in most cases not solvable analytically. Presently many codes, open-source or proprietary, exist for the efficient numerical solution of this integro-differential equation. But it is always valuable to have approximate analytical solutions in order to understand the physics. For magnetic textures, the Thiele equation [38] is such a tool.

A. The Thiele equation

Suppose that (it is possible to assume that) a structure moves as a solid object, without deforming. It means that there exists a function $\vec{m}_0(\vec{r})$ such that

$$\vec{m}(\vec{r}, t) = \vec{m}_0\left(\vec{r} - \vec{R}(t)\right), \tag{6}$$

where $\vec{R}(t)$ is the position vector of the structure. This allows expressing the time derivative of magnetization

$$\frac{\partial \vec{m}}{\partial t} = -(\vec{V} \cdot \vec{\nabla})\vec{m}_0, \tag{7}$$

where $\vec{V} = d\vec{R}/dt$ is the structure's velocity vector. We then 'solve' the LLG equation in terms of the effective field, and get

$$\vec{H}_{\text{eff}} = \frac{1}{\gamma_0} \vec{m} \times \frac{\partial \vec{m}}{\partial t} + \frac{\alpha}{\gamma_0} \frac{\partial \vec{m}}{\partial t} - \frac{1}{\mu_0 M_s} \vec{m} \times \vec{T} + \lambda \vec{m}, \tag{8}$$

where the last term appears because the component of the effective field along the magnetization cannot be determined by this way.

This effective field is used to compute the force acting on the structure, due to the energy density considered. It is given by mechanics expression $\vec{F} = -dE/d\vec{R}$. We can evaluate this derivative using the definition of the effective field

$$F_i = -\frac{\partial E}{\partial R_i} = \mu_0 M_\mathrm{s} \int \vec{H}_\mathrm{eff} \cdot \frac{\partial \vec{m}}{\partial R_i} = -\mu_0 M_\mathrm{s} \int \vec{H}_\mathrm{eff} \cdot \frac{\partial \vec{m}_0}{\partial r_i}. \tag{9}$$

The next step is to put the expression Eq. 8 of the effective field into this expression of the force [Note that the unknown function λ disappears at this moment], replacing the time derivatives by space derivatives according to the rigid motion assumption Eq. 7. This gives, using the convention of summation on repeated indices and abbreviating $\partial\vec{m}/\partial r_i$ to $\partial_i\vec{m}$,

$$F_i = \frac{\mu_0 M_\mathrm{s}}{\gamma_0} \int \left(\vec{m}_0 \times V_j \partial_j \vec{m}_0\right) \cdot \partial_i \vec{m}_0 + \alpha \frac{\mu_0 M_\mathrm{s}}{\gamma_0} \int \left(V_j \partial_j \vec{m}_0\right) \cdot \partial_i \vec{m}_0 + \int \left(\vec{m}_0 \times \vec{T}\right) \cdot \partial_i \vec{m}_0. \tag{10}$$

This can be rewritten, term by term, into the Thiele balance of forces equation [38]

$$\vec{F} + \vec{F}_\mathrm{gyro} + \vec{F}_\mathrm{dissip} + \vec{F}_\mathrm{torques} = \vec{0}. \tag{11}$$

The gyrotropic force $\vec{F}_\mathrm{gyro}$ and the dissipation force $\vec{F}_\mathrm{dissip}$ are proportional to the velocity. The dissipation force can be written $F_{\mathrm{dissip},i} = -\alpha D_{ij} V_j$, where the elements D_{ij} of the dissipation matrix $\overline{\overline{D}}$ appear. The gyrotropic force can be rewritten $\vec{F}_\mathrm{gyro} = \vec{G} \times \vec{V}$ where the components of the gyrovector $\vec{G}$ are

$$G_k = -\frac{\mu_0 M_\mathrm{s}}{\gamma_0} \frac{\epsilon_{ijk}}{2} \int \left(\partial_i \vec{m}_0 \times \partial_j \vec{m}_0\right) \cdot \vec{m}_0 d^3\vec{r}, \tag{12}$$

where ϵ_{ijk} is the Levi-Civita totally antisymmetric tensor. Comparison with the expression of the surface covered on the 2-dimensional sphere of Sec. III A 1 allows to see that, for a texture only varying in two dimensions (in a film of thickness h), the gyrovector has only a perpendicular component, that is directly proportional to the topological index of $\pi_2(\mathbb{S}^2)$ of the structure:

$$G_z = -\frac{\mu_0 M_\mathrm{s}}{\gamma_0} 4\pi h N_{\pi_2(\mathbb{S}^2)}. \tag{13}$$

This relation, together with the Thiele balance of forces equation, constitute the basis of the link between the topology of magnetic structures and their dynamics. Note that it singles out the $\pi_2(\mathbb{S}^2)$ topology. For example, for a pure XY model where $\vec{m}$ belongs to a plane, the gyrovector is automatically zero: Heisenberg spins are required.

B. Applications of the Thiele equation

The Thiele equation applies to a great variety of situations, much beyond its original scope of describing the steady-state motion of magnetic bubbles in bubble garnet films, as a function of the structure of their walls.

1. *Steady-state motion of domain walls*

Consider a one-dimensional domain wall, i.e. magnetization is a sole function of the x coordinate. The gyrovector is zero (this can be seen by analysis, from Eq. 13, or from the fact that a curve covers no surface on the unit sphere). Driving the domain wall by an easy axis field H, the steady state dynamics is simply given by $\vec{F} + \vec{F}_\mathrm{dissip} = \vec{0}$. If the wall is a 180° wall, the force per unit domain wall surface under an easy axis field is along the wall normal (x), and reads $F_x = 2\mu_0 M_\mathrm{s} H$. The dissipation matrix has only an xx element. The balance of forces thus reads $2\mu_0 M_\mathrm{s} H = \alpha D_{xx} V$. We therefore recover the well-known steady-state dynamics equation $V = (\gamma_0 \Delta_\mathrm{T}/\alpha)H$, in which instead of the Bloch wall width parameter Δ appears the so-called Thiele domain wall width Δ_T given by [39]

$$\frac{2}{\Delta_\mathrm{T}} = \int \left(\frac{d\vec{m}}{dx}\right)^2 dx. \tag{14}$$

This relation is valid whatever the profile of the domain wall. It explains why, remarkably, vortex walls in nanowires move more slowly than transverse walls under an easy axis field [40, 41], even if their lateral extent is larger. Indeed, the large magnetization gradient around the vortex core leads to a smaller Δ_T.

2. Dynamical deflection of topological structures

When discussing regular structures, we have seen the $\pi_2(\mathbb{S}^2)$ topological solitons of integer topological index for uniform boundary conditions, and the solitons with non-integer index in the case of non-uniform boundary conditions (in simple terms, the skyrmion on the one hand, the vortex and the VBL on the other hand). Consequently, these structures have a non-zero gyrovector. Hence, when moving at a velocity $\vec{V}$, the balance of forces includes the gyrotropic force $\vec{F}_{\text{gyro}} = \vec{G} \times \vec{V}$, by construction transverse to the velocity. As in the two-dimensional case the gyrovector is along the film normal, the velocity and the gyrotropic force are in the film plane, and orthogonal.

This phenomenon has been known since the invention of the Thiele equation, first in the field of bubble garnet films [38, 39], and then in the field of vortex dynamics [42], under the name of gyrotropic force (to which a gyrotropic deflection is associated). In the context of skyrmions, the effect has been called 'skyrmion Hall effect'. The derivation of the Thiele equation shows that the effect is intrinsic to the magnetization dynamics, independent of the stimulus used to drive the texture: it exists in insulators as well as in metals, or when the structure is driven by field or by electrical current. Thus, the description of this effect as due to Newton's action-reaction law in the case of current-driven motion, because of the electron deflection by the topological Hall effect [43], is misleading.

In the case of bubbles, their skew propagation with respect to an applied field gradient has been used to identify the state of the bubble, i.e. the number and type of VBLs present in the bubble's domain wall [27]. The reversal of the gyrotropic force on the VBL as its core magnetization was flipped has been observed by real time magneto-optical imaging [44]. Similarly, for vortices the sign of the gyrotropic force has been imaged in real time, as well as its reversal upon flipping the vortex core polarity [45].

3. Topological Brownian motion

The Thiele equation can be used to describe the Brownian motion, within the Langevin model where random forces, with an autocorrelation fixed by the fluctuation-dissipation theorem, are used to represent thermal agitation [46]. In the case of magnetism, white-noise random magnetic fields are introduced, which by the integral expression Eq. 10 lead to random forces on the structure. Solving the Thiele equation for the velocity vector, and performing the statistical average results in a diffusion constant $\mathcal{D}$ (leading to average quadratic displacements $< X^2(t) >=< Y^2(t) >= 2\mathcal{D}t$ after a time t) given by

$$\mathcal{D} = k_{\text{B}}T \frac{\alpha D}{G^2 + (\alpha D)^2}, \tag{15}$$

where $D = D_{xx} = D_{yy}$ for a revolution-symmetric structure is the dissipation matrix diagonal element, and G the gyrovector z component [47]. The relation agrees with the Einstein relation $\mathcal{D} = k_{\text{B}}T\mu$ with $\mu = V/F$ the viscous mobility.

This expression shows that, at low damping, the diffusion of topological structures ($G \neq 0$) is completely different from the diffusion of non-topological structures ($G = 0$). Recent experiments on skyrmions [48] indicate however that, with the present samples quality, this intrinsic diffusion regime is masked by much slower skyrmions trapping and escape processes.

V. TOPOLOGY VERSUS ENERGETIC STABILITY

By definition, a topological soliton cannot be erased (a special case of transformation to another topologically different structure) by a continuous deformation of the magnetization. This is sometimes called 'topological protection'. But does it mean that this structure cannot be erased at all ? The answer is No as we have seen: erasing this soliton requires breaking the continuity by creation of a topological defect (either by having a topological defect enter from one edge of the sample, or by creating a pair of topological defects with opposite topological indices within the sample). We have moreover seen that the Bloch point, the only topological defect of Heisenberg spins, living in 3D space, has a finite energy even in (almost everywhere, mathematically speaking) continuous micromagnetics.

So the physical answer is that, in order to erase a topological soliton, a finite energy barrier has to be overcome. And the only physical question left is how large this barrier is: by the Arrhenius law this tells us if the structure is stable on the relevant timescale (the experiment interaction time, the lifetime of a storage device, our life, the lifetime of Earth, etc.).

We describe below some cases where this erasure process has been observed, and the associated barrier evaluated.

A. The collapse of magnetic bubbles

In the magnetic bubble memory [27, 49, 50], the information 1/0 is coded by the presence/absence of a cylindrical magnetic domain, called 'bubble'. To write and rewrite information, bubbles have therefore to be created and destroyed, at higher than

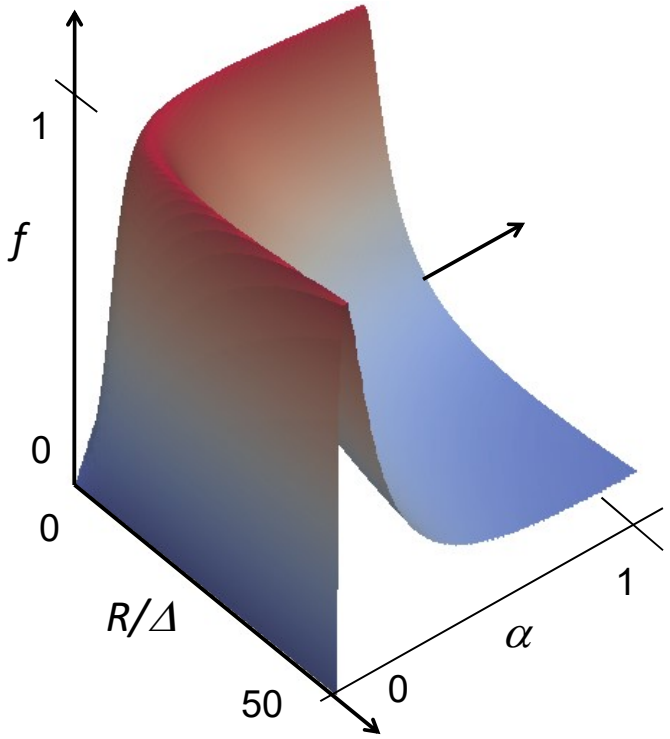

FIG. 10. The diffusion constant of a skyrmion, divided by temperature and by atomic numerical factors, is plotted in perspective view as a function of skyrmion radius R (normalized to the domain wall width parameter Δ), and Gilbert damping constant α. The crest obeys $R\alpha = \Delta$. Above this crest line, the normal behavior where diffusivity decreases as damping increases is observed. Below the crest line, the 'topological diffusion' dominates. Adapted from Ref. [47].

MHz rates. To make things worse, the bubbles used are of the topological type ($S = 1$ winding number), because these propagate faster as no VBLs slow down their motion (think of the Thiele domain wall width, see Eq. 14).

Experimentally, one characteristic of a bubble material is the so-called collapse field, above which no bubbles exist (except those pinned at structural defects, which are very rare and optically visible by strain-induced birefringence). Therefore, the 'topological protection' has never been mentioned in this context. Moreover, the collapse field can be computed from the energy versus radius profiles, as a function of the bias field, and the value of this field is used to extract the parameters of the sample. Indeed, depending on the bias field, the bubble is stable or metastable with respect to the uniform state, and at the collapse field the local minimum in the profile disappears, at a *non-zero radius* called the collapse radius. The shape of the energy profile is given by the energies of applied field, demagnetizing field, and domain wall (for the materials used for memories, the bubble radius is much larger than the domain wall width, so that the domain wall can be treated like a mathematical surface, with a surfacic energy). The excess energy of a bubble at collapse being typically $0.1\mu_0 M_s^2 h^3$ [51], one sees that as soon as $h > 3\Lambda$ this energy is larger than the insertion cost of a Bloch point. The bubble collapse is therefore explained by these evaluations.

Experiments revealed additionally that bubbles with significantly larger collapse fields, called hard bubbles [27, 52], exist. This was linked to the presence of many VBLs in the wall of the bubble, all with the same rotation sense so that such bubbles are skyrmions with a large topological index (values up to 100 were observed [27, 53]). The larger collapse field results from the progressive annihilation of pairs of VBLs under compression as the bubble shrinks under bias field. A winding VBL pair having a topological index of 1, it also involves a Bloch point during its annihilation.

Note that this observed stability of the VBL pairs has led to the concept of a Bloch line memory [54], in which the writing process of a VBL pair, necessarily discontinuous, was appropriately called Bloch point writing [55].

B. The vortex core reversal

To reverse the core of a vortex in a soft thin film, a Bloch point is required as we have seen. The vortex core reversal in such samples has been the subject of several studies.

Statically, the core polarity in NiFe disks has been observed by magnetic force microscopy, various fields being applied ex situ so as to determine a vortex core switching field [56]. The micromagnetic modelling of this experiment [11] has shown that

the Bloch point injection has to be made easier by defects; this was checked by using, instead of NiFe, an amorphous CoFeB layer in which structural defects are anticipated to be present.

The study of the dynamical switching of the vortex core polarity has revealed a quite interesting behavior. The first experiment [45] used an a.c. in-plane magnetic field to excite the resonant vortex motion in a patterned microstructure, with time-resolved transmission X-ray microscopy in stroboscopic mode for observation. As directly expected from the gyrotropic force, a rotation of the vortex core is obtained, even if the driving field is uniaxial, the rotation sense being given by the sign of the gyrovector which is, as the winding number is $S = +1$, the same as the polarity of the core. It was also observed that, upon submitting the sample to a sufficiently intense a.c. field pulse, the vortex core polarity could switch. The surprise was that, compared to the static fields of a few 100 mT required to switch the vortex core, much smaller a.c. fields (about 1 mT) were required. The second experiment [57] used an a.c. spin polarized current driving the vortex by spin-transfer torque, to obtain the same polarity switching. The micromagnetic analysis showed that a moving vortex has a distorted profile, with a dip of magnetization perpendicular component appearing next to the core [58, 59]. This dip separates into two parts when it reaches $m_z = -p$, one part annihilating with the $m_z = +p$ vortex core in a discontinuous process, leaving the other part as a $m_z = -p$ vortex core.

C. The skyrmion collapse

The annihilation of a skyrmion towards a uniform magnetic structure is equivalent to collapsing an $S = 1$ bubble. The energetics of a skyrmion is however different: whereas the bubble is stabilized by the demagnetizing field, this term is suppressed as the sample thickness goes down to one atomic monolayer. Thus, at intermediate thicknesses, both small radius skyrmions and larger radius bubbles can be stabilized [60, 61], with a continuous evolution from one structure to the other as the micromagnetic parameters are varied. This is in full agreement with topology, as both structures are equivalent in this respect. Needless to say, experiments have shown that skyrmions can be created, most directly by localized current [62, 63], and also may annihilate spontaneously [64].

In the limiting case with no long-range demagnetizing field and no applied field [65], the skyrmion is always metastable, the energy profile being impacted by a curvature term which was negligible for bubbles. Similarly to bubbles, the stability of a skyrmion requires the calculation of the energy barrier to overcome. Moreover, the prefactor τ_0 of the Arrhenius law for the skyrmion lifetime τ ($\tau = \tau_0 \exp \Delta E/(k_B T)$) needs also to be calculated. Indeed, it has been shown that it is not a constant, but varies rapidly with applied field [66].

Regarding the energy barrier, the situation is more complex than for bubbles as the maximum energy point is more difficult to find. A first approach used atomic-scale micromagnetics for a cobalt monolayer [67], together with the chain of configurations minimization method known as nudged elastic band technique. [Note that the initial Ref. [67] contains a methodological error [69], which was corrected afterwards [68].] As shown in Fig. 11, the top of the barrier is attained when the skyrmion reaches an atomic size, hence the necessity of an atomic micromagnetic model. The precise value of the energy barrier is found to depend on all energy terms, even if it duly increases when the Dzyaloshinskii-Moriya exchange term increases, as expected. In fact, based on the Belavin-Polyakov theorem [70] stating that the exchange energy of a structure has a minimum value fixed by the $\pi_2(\mathbb{S}^2)$ topological index, a fair estimation of the energy maximum is this exchange energy limit [60]. The difficulty of the energy barrier evaluation is then transferred to the calculation of the skyrmion energy relative to that of a uniform background. This is exemplified in Fig. 14

In the numerical calculation, it is notable that the configuration with the maximum energy is not realized when the skyrmion number is just 1/2, but close to that value. Regarding this 1/2 value, one ought to realize that the definition of the topological index for atomic micromagnetics, which is fundamentally discrete, is problematic. The approach chosen [71] is to keep the geometrical signification of this index, the surface covered on the sphere being evaluated as the sum of the area of all spherical triangles involved (see Fig. 11). This area of a spherical triangle is always defined except when the three summits belong to a plane going through the sphere center. At this mathematical point, the topological index is both 0 and 1 depending on how the area of this triangle is counted, a situation denoted by a $\frac{1}{2}$ topological index. Going back to topological arguments, a Bloch point cannot exists in such a sample as it is one atomic layer thick, hence really two-dimensional. Nevertheless, the change from one configuration with topological index 1 to the next with index 0 can be seen as the passage of a Bloch point through the atomic monolayer.

The energy barriers obtained by this chain minimization technique were compared to dynamic atomic scale simulations including temperature-induced fluctuations, in a narrow field window where the skyrmion annihilation is visible. In such conditions, the two determinations of the energy barrier were in agreement.

Note finally that, as the skyrmion energy at collapse depends sensitively on exchange, more complex calculations incorporating many-neighbors exchange interactions have predicted non negligible changes of the this barrier [72]. This might be a path to designing materials with atomic and electronic structures more favorable to skyrmion stability.

VI. CONCLUSION AND PERSPECTIVES

This chapter has tried to expose all the directions along which topology contributes to our understanding of the magnetic structures, be it in statics or in dynamics. As topology rests on the assumption of continuity and matter is fundamentally discontinuous, it might be tempting to dismiss all topology arguments. However, as the main energy term in ferromagnets is the exchange energy, which promotes continuity, applying topology to magnetic structures is justified. In this usage, the guide is to consider mathematics as a tool, and keep a physical approach.

Along this chapter, we have seen that the machinery of topology can be applied with profit in the description of the statics of magnetic textures, and of their transformations, with all the possible homotopy groups for spins with various degrees of freedom being involved. For the intrinsic effect of topology on magnetization dynamics, however, only the full-fledged spin with three components is relevant. This singles out the $\pi_2(\mathbb{S}^2)$ homotopy group, and consequently the magnetic skyrmion, as well as the associated merons, the magnetic vortex and the vertical Bloch line.

As new types of samples are invented, the arguments exposed here can be extended as needed. This applies also to more complex magnetic orders.

VII. ACKNOWLEDGEMENTS

This chapter is based on a tutorial talk delivered at the 61st Annual Conference on Magnetism and Magnetic Materials (New Orleans (USA), 31/10-04/11/2016), for which the presenter (A.T.) is thankful to the conference chairpersons. A.T. thanks F. Piéchon for communicating Refs. [20, 21].

---

[1] M. Kléman, *Points, Lines and Walls* (J. Wiley, Chichester, 1983)
[2] A. Hatcher, *Algebraic Topology* (Cambridge University Press, Cambridge, 2002). Online available at http://www.math.cornell.edu/~hatcher
[3] H.B. Braun, Adv. Phys. **61**, 1 (2012)
[4] W.F. Brown, Jr., *Micromagnetics* (Interscience Publishers, New York, 1963)
[5] A. Hubert, R. Schäfer, *Magnetic Domains* (Springer Verlag, Berlin, 1998)
[6] J. Friedel, *Dislocations* (Pergamon Press, London, 1964)
[7] G. Toulouse, M. Kléman, J. Physique Lettres **37**, L149 (1976)
[8] N.D. Mermin, Rev. Mod. Phys. **51**, 591 (1979)
[9] E. Feldtkeller, Z. angew. Phys. **19**, 530 (1965). English translation: IEEE. Trans. Magn. vol. 53, 0700308 (2017)
[10] W. Döring, J. Appl. Phys. **39**, 1006 (1968)
[11] A. Thiaville, J.M. García, R. Dittrich, J. Miltat, T. Schrefl, Phys. Rev. B **67**, 094410 (2003)
[12] J. Reinhardt, Int. J. Magn. **5**, 263 (1973)
[13] S.K. Kim, O. Tchernyshyov, Phys. Rev. B **88**, 174402 (2013)
[14] J.M. Kosterlitz, D.J. Thouless, J. Phys. C: Solid State Phys. **6**, 1181 (1973)
[15] H.R. Trebin, Adv. Phys. **31**, 195 (1982)
[16] M. Kläui, J. Phys.: Condens. Matter **20**, 313001 (2008)
[17] H. Hopf, Math. Ann **104**, 637 (1931)
[18] P.J. Ackerman, I.I. Smalyukh, Nat. Mater. **16**, 426 (2017)
[19] J.S.B. Tai, I.I. Smalyukh, Phys. Rev. Lett. **121**, 187201 (2018)
[20] F. Wilczek, A. Zee, Phys. Rev. Lett. **51**, 2250 (1983)
[21] D.L. Deng, S.T. Wang, C. Shen, L.M. Duan, Phys. Rev. B **88**, 201105(R) (2013)
[22] E. Feldtkeller, H. Thomas, Phys. kondens. Materie **4**, 8 (1965)
[23] G. de Loubens, A. Riegler, B. Pigeau, F. Lochner, F. Boust, K.Y. Guslienko, H. Hurdequint, L.W. Molenkamp, G. Schmidt, A.N. Slavin, V.S. Tiberkevich, N. Vukadinovic, O. Klein, Phys. Rev. Lett. **102**, 177602 (2009)
[24] O. Tchernyshyov, G.W. Chern, Phys. Rev. Lett. **95**, 197204 (2005)
[25] G.W. Chern, H. Youk, O. Tchernyshyov, J. Appl. Phys. **99**, 08Q505 (2006)
[26] D.J. Clarke, O.A. Tretiakov, G.W. Chern, Y.B. Bazaliy, O. Tchernyshyov, Phys. Rev. B **78**, 134412 (2008)
[27] A.P. Malozemoff, J.C. Slonczewski, *Magnetic Domain Walls in Bubble Materials* (Academic Press, New York, 1979)
[28] S. Konishi, IEEE Trans. Magn. **19**, 1838 (1983)
[29] P. Milde, D. Köhler, J. Seidel, L.M. Eng, A. Bauer, A. Chacon, J. Kinderwater, S. Mühlbauer, C. Pfleiderer, S. Buhrandt, C. Schütte, A. Rosch, Science **340**, 1076 (2013)
[30] F.N. Rybakov, A.B. Borisov, S. Blügel, N.S. Kiselev, Phys. Rev. Lett. **115**, 117201 (2015)
[31] L. Landau, E. Lifshitz, Phys. Z. Sowjetunion **8**, 153 (1935)
[32] T.L. Gilbert, Phys. Rev. **100**, 1243 (1955). (abstract only)
[33] A. Thiaville, Y. Nakatani, J. Miltat, Y. Suzuki, Europhys. Lett. **69**, 990 (2005)

[34] A. Thiaville, S. Rohart, É. Jué, V. Cros, A. Fert, Europhys. Lett. **100**, 57002 (2012)
[35] T.L. Gilbert, Formulation, foundations and applications of the phenomenological theory of ferromagnetism. Ph.D. thesis, Illinois Institute of Technology, Chicago (1956). Partly reprinted in IEEE. Trans. Magn. 40, 3443-3449 (2004).
[36] G.S.D. Beach, M. Tsoi, J.L. Erskine, J. Magn. Magn. Mater. **320**, 1272 (2008)
[37] A. Manchon, J. Zelezný, I.M. Miron, T. Jungwirth, J. Sinova, A. Thiaville, K. Garello, P. Gambardella, Rev. Mod. Phys. **91**, 035004 (2019)
[38] A.A. Thiele, Phys. Rev. Lett. **30**, 230 (1973)
[39] A.A. Thiele, J. Appl. Phys. **45**, 377 (1974)
[40] Y. Nakatani, A. Thiaville, J. Miltat, J. Magn. Magn. Mater. **290-291**, 750 (2005)
[41] L. Thomas, M. Hayashi, X. Jiang, R. Moriya, C. Rettner, S. Parkin, Nature **443**, 197 (2006)
[42] D.L. Huber, J. Appl. Phys. **53**, 1899 (1982)
[43] N. Nagaosa, Y. Tokura, Nat. Nanotechnol. **8**, 899 (2013)
[44] A. Thiaville, J. Miltat, Europhys. Lett. **26**, 1006 (1994)
[45] B. van Waeyenberge, A. Puzic, H. Stoll, K.W. Chou, T. Tyliszczak, R. Hertel, M. Fähnle, H. Brückl, K. Rott, G. Reiss, I. Neudecker, D. Weiss, C.H. Back, G. Schütz, Nature **444**, 461 (2006)
[46] W.F. Brown, Jr., Phys. Rev. **130**, 1677 (1963)
[47] J. Miltat, S. Rohart, A. Thiaville, Phys. Rev. B **97**, 214426 (2018)
[48] J. Zázvorka, F. Jakobs, D. Heinze, N. Keil, S. Kromin, S. Jaiswal, K. Litzius, G. Jakob, P. Virnau, D. Pinna, K. Everschor-Sitte, L. Rózsa, A. Donges, U. Nowak, M. Kläui, Nat. Nanotechnol. **14**, 658 (2019)
[49] A.H. Bobeck, I. Danylchuk, J.P. Remeika, L.G. van Uitert, E.M. Walters, *Proceedings of the International Conference on Ferrites 1970* (U. of Tokyo Press, Tokyo, 1971), p. 361
[50] A.H. Eschenfelder, *Magnetic bubble technology*, *Springer series in solid state science*, vol. 14 (Springer, Berlin, 1980)
[51] A.A. Thiele, Bell Syst. Tech. J. **48**, 3287 (1969)
[52] W.J. Tabor, A.H. Bobeck, G.P. Vella-Coleiro, A. Rosencwaig, Bell Syst. Tech. J. **51**, 1427 (1972)
[53] K. Kobayashi, N. Nishida, Y. Sugita, J. Phys. Soc. Japan **34**, 555 (1973)
[54] S. Konishi, K. Matsuyama, I. Chida, S. Kubota, H. Kawahara, M. Ohbo, IEEE Trans. Magn. **20**, 1129 (1984)
[55] Y. Maruyama, T. Ikeda, R. Suzuki, IEEE Transl. J. Magn. Japan **4**, 730 (1989)
[56] T. Okuno, K. Shigeto, T. Ono, K. Mibu, T. Shinjo, J. Magn. Magn. Mater. **240**, 1 (2002)
[57] K. Yamada, S. Kasai, Y. Nakatani, K. Kobayashi, H. Kohno, A. Thiaville, T. Ono, Nature Mater. **6**, 270 (2007)
[58] K.W. Chou, A. Puzic, H. Stoll, D. Dolgos, G. Schütz, B. Van Waeyenberge, A. Vansteenkiste, T. Tyliszczak, G. Woltersdorf, C.H. Back, Appl. Phys. Lett. **90**, 202505 (2007)
[59] V. Novosad, F.Y. Fradin, P.E. Roy, K.S. Buchanan, K.Y. Guslienko, S.D. Bader, Phys. Rev. B **72**, 024455 (2005)
[60] F. Büttner, I. Lemesh, G.S.D. Beach, Sci. Rep. **8**, 4464 (2018)
[61] A. Bernand-Mantel, L. Camosi, A. Wartelle, N. Rougemaille, M. Darques, L. Ranno, SciPost Phys. **4**, 027 (2018)
[62] N. Romming, C. Hanneken, M. Menzel, J.E. Bickel, B. Wolter, K. von Bergmann, A. Kubetzka, R. Wiesendanger, Science **341**(6146), 636 (2013). doi:10.1126/science.1240573
[63] A. Hrabec, J. Sampaio, M. Belmeguenai, I. Gross, R. Weil, S.M. Chérif, A. Stashkevich, V. Jacques, A. Thiaville, S. Rohart, Nat. Commun. **8**, 15765 (2017)
[64] S. Woo, K. Litzius, B. Krüger, M.Y. Im, L. Caretta, K. Richter, M. Mann, A. Krone, R.M. Reeve, M. Weigand, P. Agrawal, I. Lemesh, M.A. Mawass, P. Fischer, M. Kläui, G.S.D. Beach, Nat. Mater. **15**, 501 (2016)
[65] S. Rohart, A. Thiaville, Phys. Rev. B **88**, 184422 (2013)
[66] L. Desplat, D. Suess, J.V. Kim, R.L. Stamps, Phys. Rev. B **98**, 134407 (2018)
[67] S. Rohart, J. Miltat, A. Thiaville, Phys. Rev. B **93**, 214412 (2016)
[68] S. Rohart, J. Miltat, A. Thiaville, Phys. Rev. B **95**, 136402 (2017)
[69] P. Bessarab, Phys. Rev. B **95**, 136401 (2017)
[70] A.A. Belavin, A.M. Polyakov, JETP Lett. **22**, 245 (1975)
[71] B. Berg, M. Lüscher, Nucl. Phys. B **190**, 412 (1981)
[72] S. von Malottki, B. Dupé, P.F. Bessarab, A. Delin, S. Heinze, Sci. Rep. **7**, 12299 (2017)

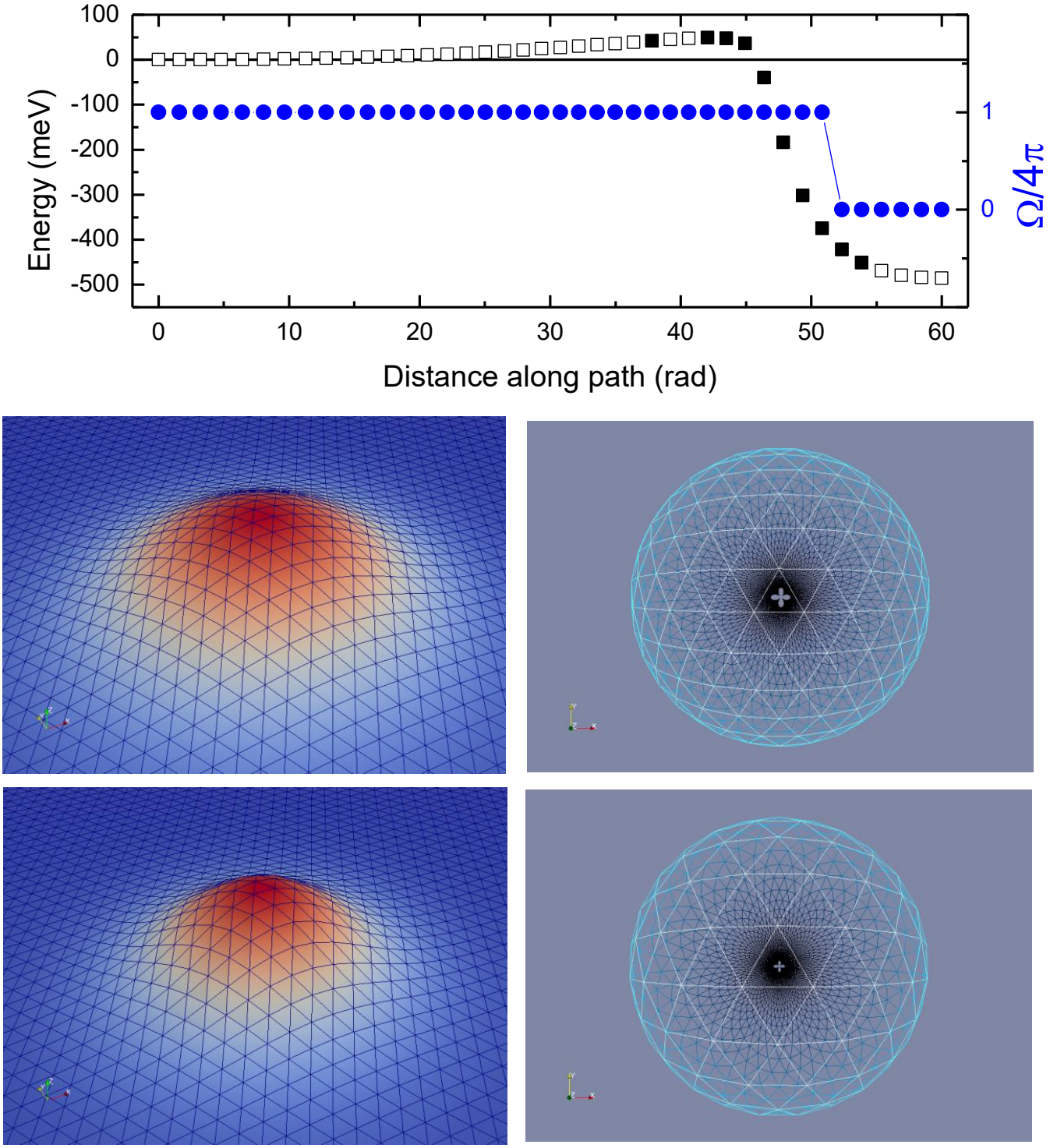

FIG. 11. Calculations were performed using the nudged elastic band technique, with 41 linked configurations, in an atomic micromagnetic code [67, 68]. The DMI energy per Co-Co bond is 1.8 meV. (top) Variation of total energy, and topological number with number of the configuration along the path (the path is shown by its length in configuration space, and the full squares correspond to the images shown in the rest of the figure) (bottom) Dual representation of chosen configurations along the path, here with number 26 and 29 (continued on the next pages with numbers 30-33, and 34-37). For each configuration, the left column shows a real space view, with the surface height and color displaying the perpendicular m_z component (red: positive; blue: negative). The triangular mesh corresponds to the atomic lattice and the nearest-neighbour bonds. The right column depicts the image of the configuration on the unit sphere $\mathbb{S}^2$, as seen from the North direction. The color of the nearest neighbor bonds expresses the latitude on the sphere (white: North, black: South, blue: Equator).

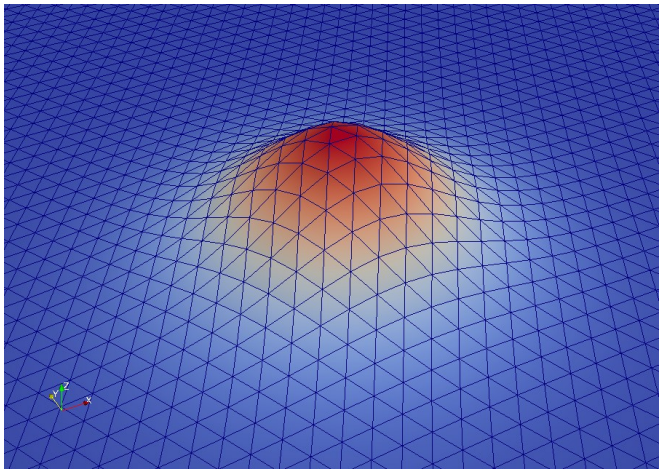

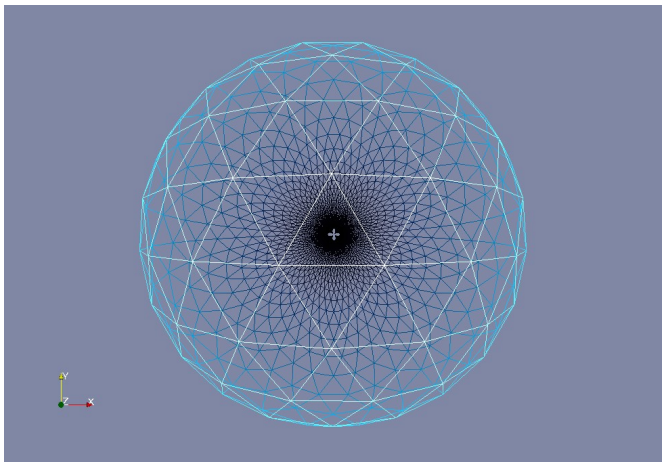

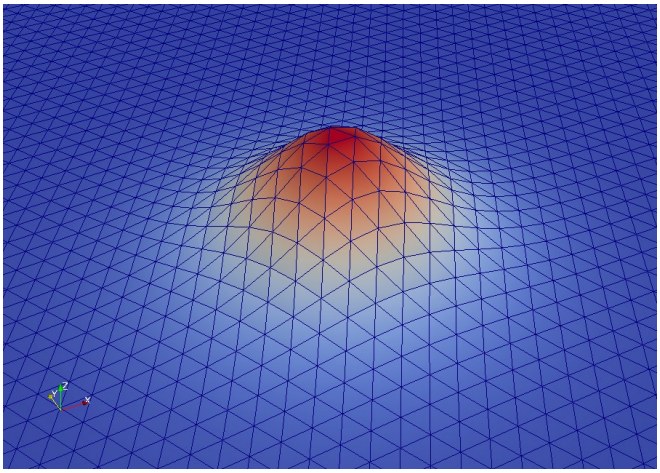

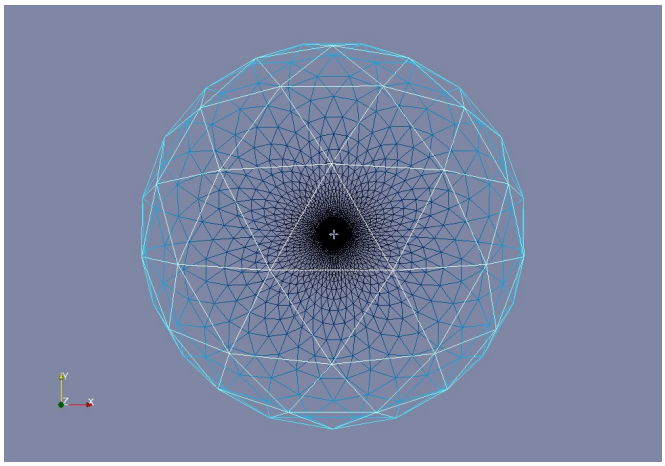

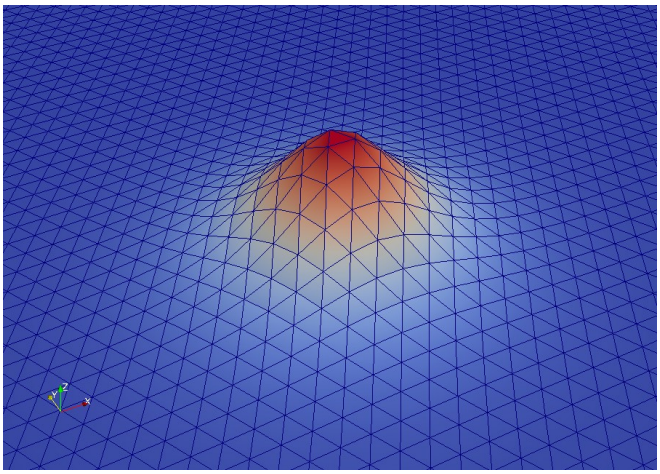

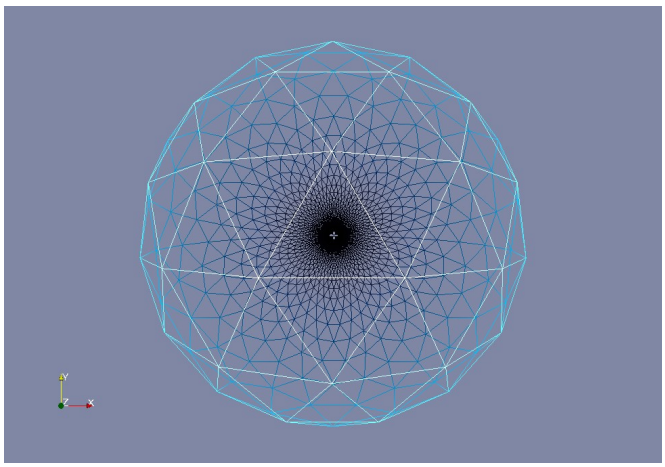

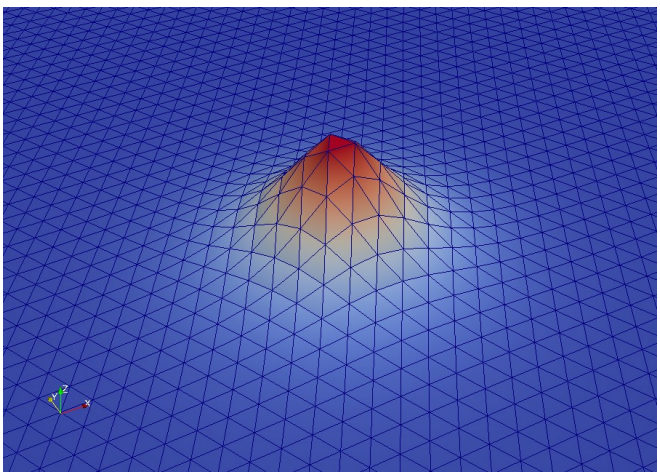

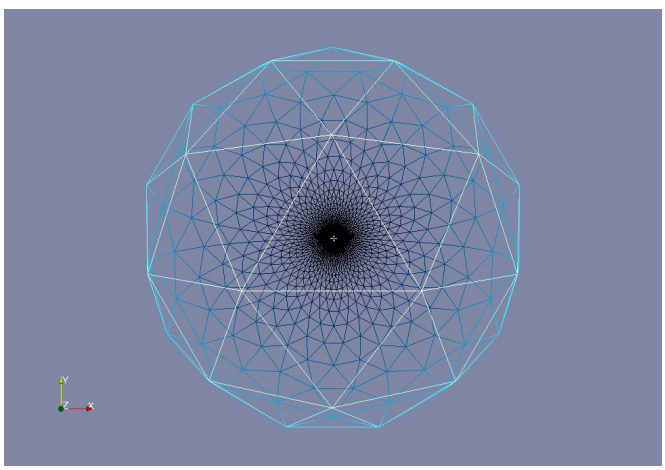

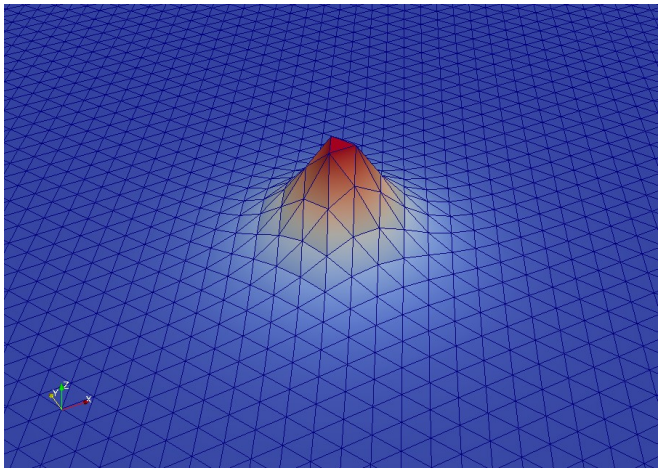

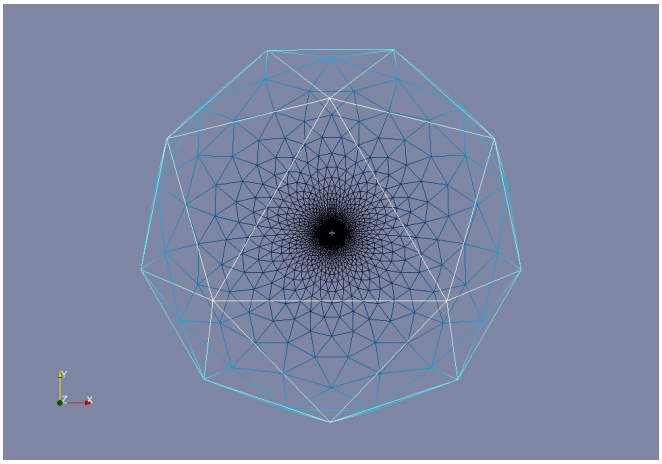

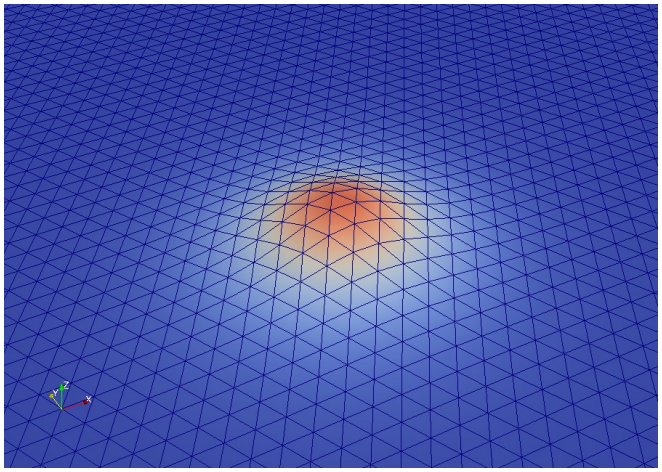

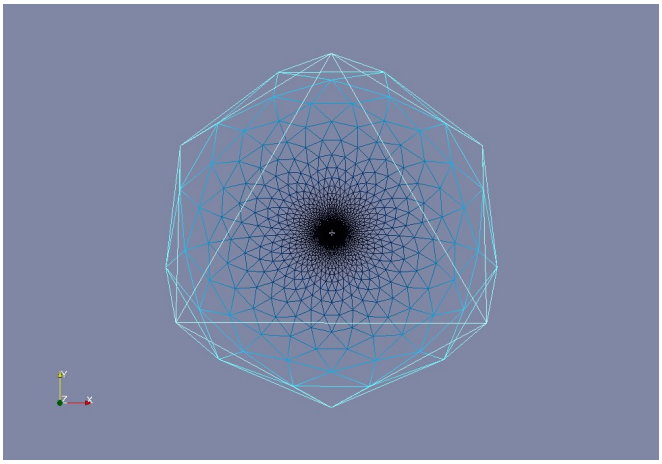

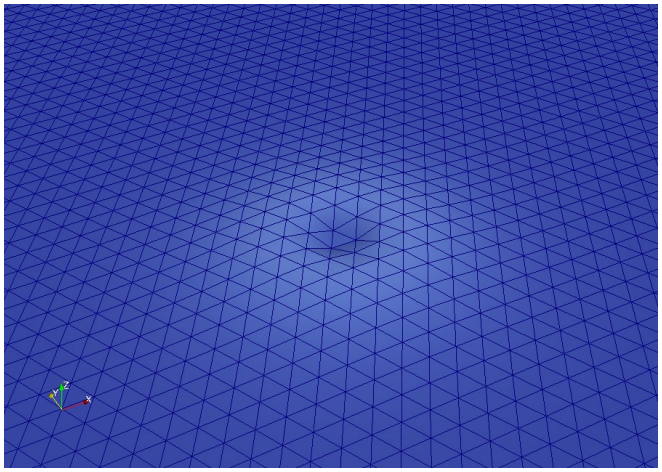

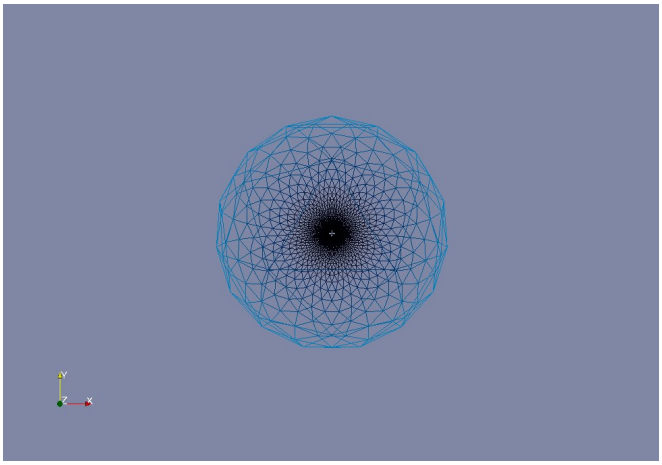

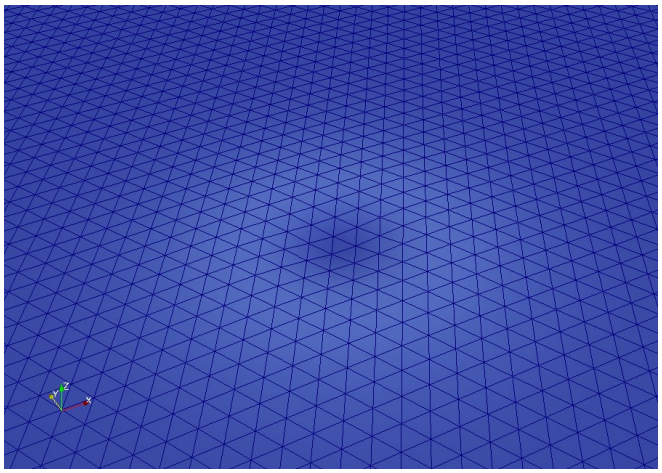

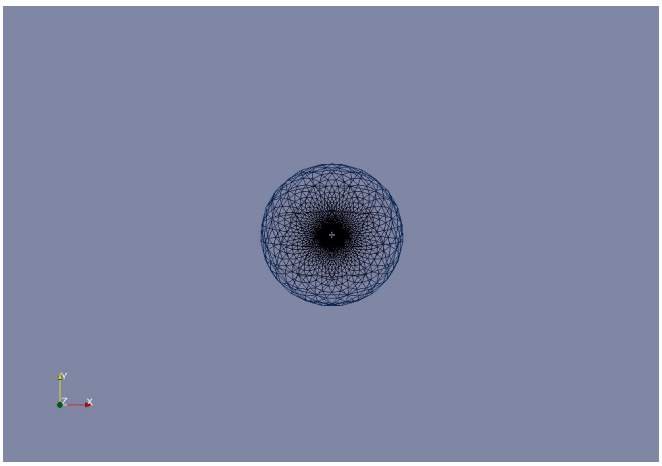

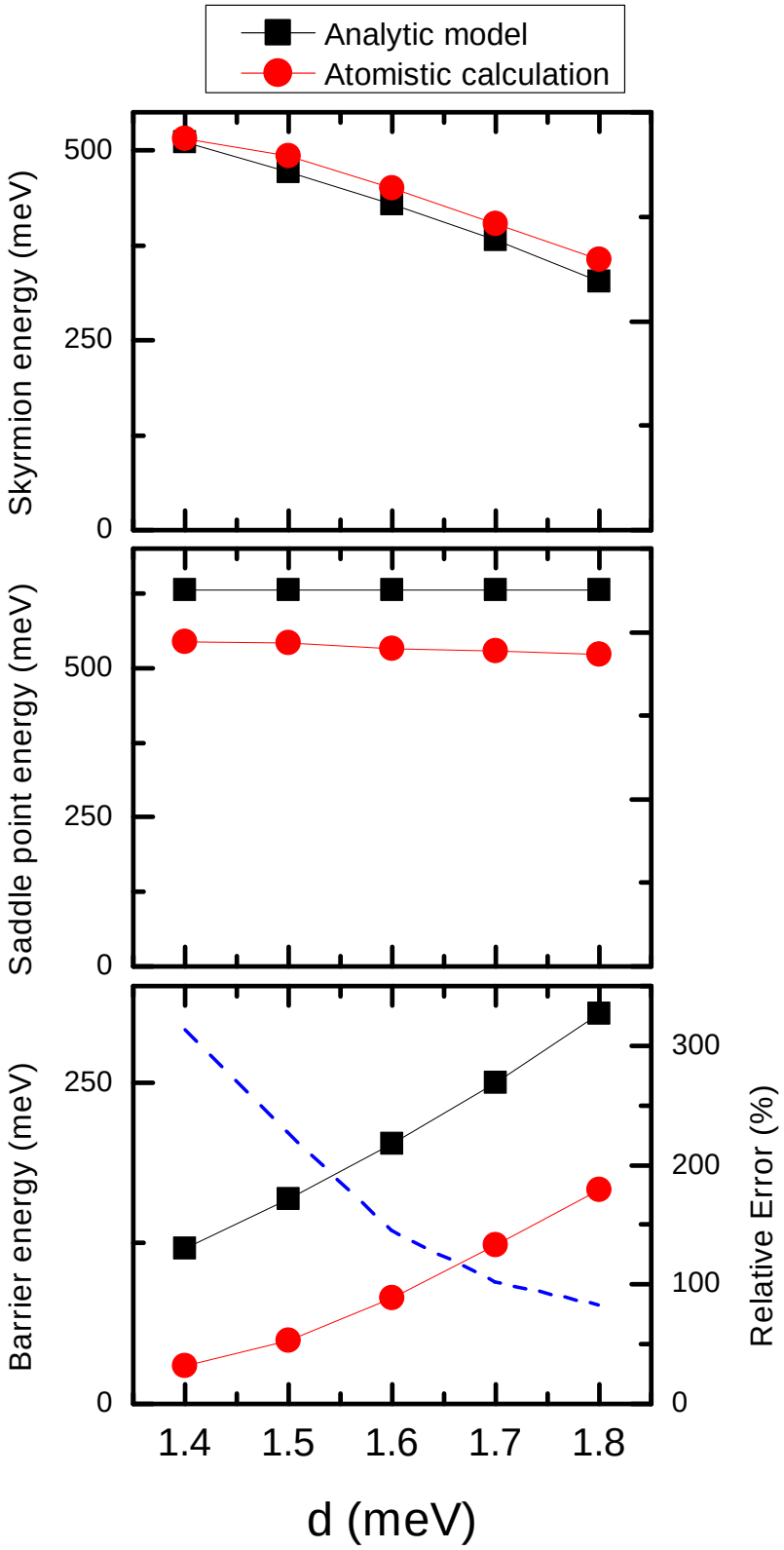

FIG. 14. For a cobalt monoatomic layer, and as a function of the strength of the bond DMI, the analytical model and the atomic micromagnetic model results are compared. (top) skyrmion absolute energy, (middle) saddle point absolute energy and, (bottom) resulting energy barrier. One sees that, even if the absolute energies are fairly described, their difference is much poorly obtained by the analytical model.